Experimental Electron Density in a Transition Metal Dimer: Metal−Metal and Metal−Ligand Bonds

Piero Macchi,* Davide M. Proserpio, and Angelo Sironi*

Contribution from the Dipartimento di Chimica Strutturale e Stereochimica Inorganica and Centro CNR-CSMTBO, Università degli Studi di Milano, Via G. Venezian 21, 20133 Milano, Italy

Received August 12, 1998

Abstract: The accurate experimental electron density distribution of $Co_2(CO)_6(AsPh_3)_2$ has been determined through X-ray diffraction at $T = 123$ K. Metal−metal and metal−ligand bonds have been investigated by means of deformation densities and the quantum theory of atoms in molecules. The "expected" lack of charge accumulation in the deformation density map is "contradicted" by the presence of a bond critical point and a bond path line linking the two Cobalt atoms, in agreement with theoretical predictions on similar compounds. A careful analysis of the properties of $\rho(\mathbf{r})$ at the bond critical points and of the Laplacian distribution along the bond paths has allowed the full characterization of all bonds in the title compound and, in particular, to discard the apparently straightforward classification of Co−Co as a closed-shell interaction. The radial shape of the *atomic* Laplacian makes (covalent or polar) shared interactions similar to donor−acceptor ones when at least one "heavy atom" is concerned. Thus, even if it is possible to recognize the shared character of Co−Co and As−C bonds by comparison with the donor−acceptor C−Co and As−Co interactions, this distinction is grounded on subtleties which could possibly not suffice without some a priori chemical insight.

Introduction

Most of the known transition metal dimers (and many low-nuclearity clusters) more or less conform to the 18-valence electrons rule, thus offering an experimental, indirect evidence for the "status" of bonds of many metal−metal (MM) interactions. This is particularly cogent, when the lack of bridging ligands, i.e. the presence of short "unsupported" MM contacts, straightforwardly drives chemists to speak of covalent (as in $Mn_2(CO)_{10}$) or even dative (as in $CrOs(CO)_{10}$)[1] MM bonds. Theoreticians have, however, cast some doubt on the nature of these bonds, sometimes suggesting that most of their binding energy is actually due to 1,3 M···CO interactions,[2] but a definite word about the existence of true MM bond was not achieved. The accurate electron density of a few metal dimers was also studied by X-ray diffraction,[3−5] but most of these studies were made before the quantum theory of atoms in molecules (QTAM)[6] and the multipole model[7] were common practice among crystallographers[8] and, standing on the interpretation of rather noisy deformation density (DD) maps, could not produce a clear understanding of the MM interaction. Later on, it was recognized that the major weakness of the DD approach stands principally on the difficult choice of the proper *promolecule*, a choice which is particularly delicate when the total density between the two atoms is small or when atoms have more than half-filled shells (a problem which was first observed for the F_2 molecule and came out also for C−F and O−O bonds[9] in experimental studies and could be solved only by introducing the so-called *chemical deformation densities*[10]). Density accumulations in MM bonds become somewhat visible only by using *fragment deformation maps*.[11,12]

The QTAM apparently offers a better and less ambiguous theoretical understanding of MM interactions, providing a distinction between unsupported (where a MM bond path is found) and ligand bridged (without MM bond) species.[13,14] QTAM has been recently used for the interpretation of the experimental charge density of $Mn_2(CO)_{10}$, confirming the presence of a bond critical point between the two metal atoms,[15] but we think that there is still more knowledge to be extracted

* E-mail: piero@csmtbo.mi.cnr.it; angelo@csmtbo.mi.cnr.it.

(1) Davis, H. B.; Einstein, F. W. B.; Glavina, P. G.; Jones, T.; Pomeroy, R. K.; Rushman, P. *Organomet.* **1989**, *8*, 1030−1039.

(2) Brown, D. A.; Chambers, W. J.; Fitzpatrick, N. J.; Rawilson, R. M. *J. Chem. Soc. A* **1971**, 720−725.

(3) Martin, M.; Rees, B.; Mitschler, A. *Acta Crystallogr.* **1982**, *B38*, 6−15.

(4) (a) Clemente, D. A.; Rees, B.; Bandoli, G.; Cingi Biagini, M.; Reiter, B.; Herrmann, W. A. *Angew. Chem., Int. Eng. Ed.* **1981**, *20*, 887−888. (b) Clemente, D. A.; Cingi Biagini, M.; Rees, B.; Herrmann, W. A. *Inorg. Chem.* **1982**, *21*, 3741−3749. (c) Mitschler, A.; Rees, B.; Lehmann, M. S. *J. Am. Chem. Soc.* **1978**, *100*, 3390−3397.

(5) Leung, P. C.; Coppens, P. *Acta Crystallogr.* **1983**, *B39*, 535−542, in this paper the multipolar model was adopted, thus model deformation density maps could be produced.

(6) Bader, R. F. W. Atoms in Molecules: a quantum theory. *International series of monographs on chemistry*, Vol. 22; Oxford University Press: Oxford, U.K., 1990.

(7) (a) Hansen, K. H.; Coppens, P. *Acta Crystallogr.* **1978**, *A34*, 909−921. (b) Stewart, R. F. *Acta Crystallogr.* **1976**, *A32*, 565−574.

(8) Coppens, P. X-Ray charge densities and chemical bonding. *IUCr Texts on Crystallography*; Oxford University Press: Oxford, U.K., 1997.

(9) Kunze, K. L.; Hall, M. B. *J. Am. Chem. Soc.* **1986**, *108*, 5122−5127.

(10) Schwarz, W. H. E.; Ruedenberg, K.; Mensching, L. *J. Am. Chem. Soc.* **1989**, *111*, 6926−6933. Mensching, L.; Von Niessen, W.; Valtanzanos, P.; Ruedenberg, K.; Schwarz, W. H. E. *J. Am. Chem. Soc.* **1989**, *111*, 6933−6941.

(11) (a) Low, A. A.; Kunze, K. L.; MacDougall, P. J.; Hall, M. B. *Inorg. Chem.* **1991**, *30*, 1079−1086. (b) Hall, M. B. *Electron Distribution and the Chemical Bond*; Coppens, P., Hall, M. B., Eds.; Plenum: New York, 1982.

(12) Heijser, W.; Baerends, E. J.; Ros, P. *Discuss. Faraday Soc. (Symp.)* **1980**, *14*, 211−234.

(13) (a) MacDougall, P. J. Ph.D. Thesis, McMaster University, 1990. (b) MacDougall, P. J.; Hall, M. B. *Trans. Am. Crystallogr. Assoc.* **1990**, *26*, 105−123.

(14) Bo, C.; Sarasa, J. P.; Poblet, J. M. *J Phys. Chem.* **1993**, *97*, 6362−6366.

10.1021/ja982903m CCC: $15.00
Published on Web 12/10/1998

by means of QTAM analysis of experimental densities in the realm of metal clusters. This can be achieved provided that one takes into account (a) the copresence of contracted 3d and diffuse 4s electrons in the valence shell, (b) the large total number of core electrons, and (c) the huge atomic sizes (features which all leave recognizable traces in the Laplacian distribution). For this reason we discuss here a complete X-ray diffraction study on a novel unsupported dimeric species, namely $Co_2(CO)_6(AsPh_3)_2$, where the $AsPh_3$ ligand has been intentionally chosen to allow a comparison between the different behavior of two different heavy atoms and, eventually, between the "covalent" Co−Co and the "dative" As−Co bonds.

Experimental Section

$Co_2(CO)_6(AsPh_3)_2$ crystallizes in the $R\bar{3}$ space group, and lying about a $\bar{3}$ symmetry element, it has an S_6 symmetry at room temperature.[16] The molecule contains two trigonal bipyramidal cobalt atoms linked by an unsupported Co−Co bond along the axial direction. The two $AsPh_3$ ligands are bonded in the remaining axial sites, while the terminal CO's are equatorially bounded and markedly bent away from the $AsPh_3$ ligands, i.e. toward the opposite Co atom (C−Co−Co ≈ 86°). The title compound undergoes a solid-state phase transition[16] at $T_c = 206$ K: the intramolecular inversion center is lost in the low-temperature phase (reducing the symmetry to C_3) and the **c** cell axis is doubled, while the space group is unchanged.[17] The major conformational changes occurring *upon* the phase transformation (down to ca. 140 K) are the rotation of the two $Co(CO)_3$ and of the two $AsPh_3$ moieties about their 3-fold axes and the rotation of the phenyls about the As−C bond.[16]

Data Collection and Reduction. A violet crystal (dimension 0.20 × 0.15 × 0.15 mm) was mounted in air on a SMART-CCD diffractometer, equipped with a N_2 gas stream low-temperature device, and cooled to 123 K in 1 h.[18] The performances of this area detector for accurate electron density determination have been accurately investigated over the last 2 years with positive results;[19] the experimental procedures here adopted have been optimized during two previous works.[19a,b] Graphite-monochromatized Mo Kα ($\lambda = 0.710\,73$ Å) radiation was used (0.5 mm collimated) with a generator working at 45 kV and 40 mA. Cell parameters were initially determined by least-squares fittings over 212 reflections contained in 45 frames ($0 < \theta < 37°$) collected in three different ω regions. The 49 617 intensities were collected with the ω-scan method ($\Delta\omega = 0.3°$) within the limits $0 < 2\theta < 100°$ (maximum $\sin\theta/\lambda = 1.06$ Å^{-1}). The detector was kept at 2.93(1) cm from the sample;[20] four sets of 500 frames each (60 s per frame) within $0 < 2\theta < 75°$ (detector arm at $\theta_d = 30°$) and two sets of 330 frames (120 s. per frame) in the limits $25 < 2\theta < 100°$ ($\theta_d = 60°$) were then collected. The intensity spots partially obscured by the beamstop were detected and rejected before applying an analytical absorption correction (XPREP).[21] Recollection of the first 50 frames did not show any significant crystal decay.

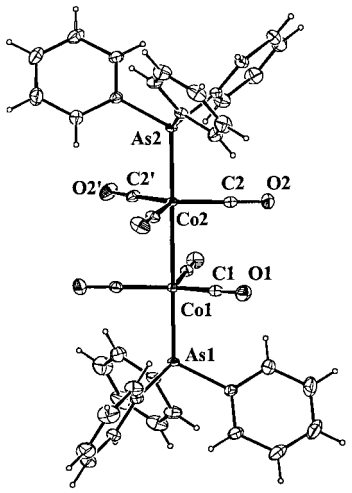

Figure 1. View of $Co_2(CO)_6(AsPh_3)_2$ molecular structure; ellipsoids are drawn at the 50% probability level.

Refinements. An initial spherical atom refinement (SHELX97)[21] was carried out to determine accurately positions and anisotropical thermal parameters for non-hydrogen atoms (using high-order data only); then H atoms were accurately fixed using generalized scattering factors[22] for H (up to dipoles) polarized in the direction of the bonded C atoms. In all successive multipolar refinements, hydrogen coordinates were kept fixed (see Figure 1 for the molecular geometry at $T = 123$ K).

The multipolar method proposed by Hansen and Coppens[7a] was adopted. Each atom was assigned a finite multipole expansion, truncated at hexadecapolar level for Co and As (of course, since these atoms lie on the 3-fold axes, only multipoles allowed by the 3 site symmetry[23] were used), at the octupolar level for C and O and at the dipole level for H atoms (only a dipole directed toward the riding C atom was included). Core and spherical valence densities were constructed using Clementi and Roetti Hartree−Fock (HF)[24] atomic wave functions;[25] the radial functions for the deformation densities were single-ζ Slater-type orbitals for As, C, O, and H,[26] while HF radial functions were used for Co atoms. Due to the presence of a molecular pseudo-inversion center, there are pseudo-symmetrical pairs of atoms and full refinements produce some large correlation coefficients; thus, "chemical constraints" [27] on the multipolar coefficients were imposed to all these pairs of atoms but the two Co and the two As atoms (all H atoms were also constrained to have the same coefficients). The final agreement indexes are slightly worse, but correlation coefficients are much more satisfactory (all of the features described in the discussion are qualitatively similar for the "constrained" and the "unconstrained" models). A radial scaling for the spherical density was refined for each atom-type together with a scaling of the radial function for the deformation density (only for Co, κ' and κ'' were constrained to be equal). Crystal data and results of refinements are reported in Table 1.

(15) Bianchi, R.; Gervasio, G.; Marabello, D. *Chem. Commun.* **1998**, 1535−1536.

(16) Macchi, P.; Garlaschelli, L.; Martinengo, S.; Sironi, A. *Inorg. Chem.* **1998**, *37*, 6263−6268.

(17) Since this phase transition is *antiferrodistorsive* (i.e., there is a loss of translational symmetry) but *antiferroic* (the point group symmetry of the crystal is preserved), there is no formation of crystal domains upon the phase transition, thus the accurate charge density can be safely determined.

(18) The stability of the crystal under a relatively rapid cooling was already tested in the experiments carried out to study the phase transition (here however a different crystal was employed).

(19) (a) Macchi, P.; Proserpio, D. M.; Sironi, A. *J. Am. Chem. Soc.* **1998**, *120*, 1447−1455. (b) Macchi, P.; Proserpio, D. M.; Sironi, A.; Soave, R.; Destro, R. *J. Appl. Crystallogr.* **1998**, *31*, 583−588. (c) Koritsanszky, T.; Flaig, R.; Zobel, D.; Krane, H. G.; Morgenroth, W.; Luger, P. *Science* **1998**, *279*, 356−358. (d) Graafsma, H.; Svensson, S. O.; Kvick, Å. *J. Appl. Crystallogr.* **1997**, *30*, 957−962. (e) Kirschbaum, K.; Martin, A.; Pinkerton, A. A. *J. Appl. Crystallogr.* **1997**, *30*, 514−516. (f) Martin, A.; Pinkerton, A. A. *Acta Crystallogr.* **1998**, *B54*, 471−477.

(20) The primitive rhombohedral cell has $a = 12.934$ Å and $\alpha = 72.17°$; thus, this short detector−sample distance is allowed without the problem of superimposing spots.

(21) Sheldrick, G. M. *SHELX-97: a program for structure refinement*; University of Gottingen: Gottingen, Germany, 1997.

(22) (a) Stewart, R. F.; Davidson, E. R.; Simpson, W. T. *J. Chem. Phys.* **1965**, *42*, 3175−3187. (b) Stewart, R. F.; Bentley, J. Goodman, B. *J. Chem. Phys.* **1975**, *63*, 3786−3793.

(23) Kurki-Suonio, K. *Isr. J. Chem.* **1977**, *16*, 115−123.

(24) Clementi, E.; Roetti, C. *At. Data Nucl. Data Tables* **1974**, *14*, 177−478.

(25) For Co atom a $4s^23d^7$ configuration was assumed; refinements using the $4s^13d^8$ configuration showed very similar agreement indexes, but a rather unrealistic depopulation of d orbitals and redistribution of charges on ligand atoms was found. No data are available for the $3d^9$ configuration in Clementi and Roetti wave function data (ref 24); however, it seems that a populated 4s orbital is more realistic, in agreement with what was found for $Ni(COD)_2$ (ref 19a).

(26) Clementi, E.; Raimondi, L. *J. Chem. Phys.* **1963**, *38*, 2686−2689.

(27) This kind of procedure, implemented in XD, has been already adopted in ref 19a with very satisfactory results. See: (a) Tanake, K.; Elkaim, E.; Li, L.; Jue, Z. N.; Coppens, P. *J. Chem. Phys.* **1986**, *84*, 6969−6978. (b) Li, N.; Coppens, P.; Landrum, J. *Inorg. Chem.* **1988**, *27*, 482−488 (for the earlier applications of chemical constraints technique).

Table 1. Crystal Data for $Co_2(CO)_6(AsPh_3)_2$[a]

chemical formula	$C_{42}H_{30}O_6Co_2As_2$
$a = b$ (Å)	15.235(2)
c (Å)	28.446(3)
V (Å^3)	5718(1)
Z	6
crystal system	trigonal
space group	$R\bar{3}$
T (K)	123(1)
scan method	ω
frame width (deg)	0.3
no. of frames	2710
total no. of reflns (redundancy)	49617 (4.31)
no. of unique reflns (R_{int})	11511 (0.0404)
R_σ	0.053
spherical atom refinement ($I > 2\sigma(I)$)	
R_1	0.0297
wR_2	0.0448
multipolar refinement ($I > 2\sigma(I)$)	
R_1	0.0237
R_2	0.0286
R_2 (all data)	0.0357
wR_1	0.0148
wR_2	0.0285
GOF	1.04
no. of variables	347

[a] $R_{int} = \sum|F_o^2 - F_{mean}^2|/\sum F_o^2$; $R_\sigma = \sum\sigma(F_o^2)/\sum F_o^2$; $R_1 = \sum||F_o| - |F_c||/\sum|F_o|$; w$R_1 = (\sum(F_o - F_c)^2/\sum wF_o^2)^{1/2}$; $R_2 = \sum||F_o^2| - |F_c^2||/\sum|F_o^2|$; w$R_2 = (\sum(F_o^2 - F_c^2)^2/\sum wF_o^4)^{1/2}$.

The Hirshfeld rigid bond test[28] was positive for all bonds (the greatest difference between mean-square amplitudes never exceeds 1.0×10^{-3} Å) but Co−C and As−C bonds, as expected on the basis of the different atomic masses.[29]

Computational Details. All multipolar refinements were carried out using the XD software package;[30] the quantity minimized was $\epsilon = \sum w(F_o^2 - F_c^2)$ based on the 7505 reflections with $I > 2\sigma(I)$. Weights were taken as $w = 1/\sigma^2(F^2)$. Convergence was assumed when $|\delta(\epsilon)/\epsilon| = |(\epsilon_n - \epsilon_{n-1})/\epsilon| \leq 10^{-5}$ (where n is the number of the cycles). The properties of $\rho(\mathbf{r})$ and $\nabla^2\rho(\mathbf{r})$ and topological analysis were computed after transformation of the local axis system into a global system, and at each point, contributions from atoms located in a sphere of radius 6.0 Å were considered. The experimental energy densities were derived semiquantitatively as recently proposed by Abramov.[31]

A few "explorative" ab initio molecular orbital calculations at Hartree−Fock and density functional (B3LYP)[32] level were carried on GAUSSIAN94[33] using the experimental geometry of the high-temperature phase (thus in S_6 symmetry) and pseudopotential basis sets.[34] More extensive calculations, using different basis sets up to 6-311+G*, were performed on $Co_2(CO)_6(AsH_3)_2$ (the geometrical features of the $Co_2(CO)_6$ moiety were kept fixed, while only the ligand conformation was optimized). When the same basis set and method were employed, very similar topological analyses in Co−Co, Co−As, and Co−C bonds were obtained (PROAIM)[35] for $Co_2(CO)_6(AsPh_3)_2$ and $Co_2(CO)_6(AsH_3)_2$, thus allowing the comparisons proposed in Table 4 and Figure 4.

Table 2. Atomic d-Orbital Populations for the Two Independent Co Atoms (According to the Partitioning Scheme Proposed in Ref 36)

	Co1	Co2
d_{z^2}	0.65(1)	0.82(1)
d_{xz}, d_{yz}	1.82(2)	1.63(2)
$d_{x^2-y^2}$, d_{xy}	1.33(2)	1.38(2)
total d population	6.95(4)	6.82(4)

Table 3. Atomic Charges Obtained by Multipolar Refinements

atom	charge	atom	charge
As(1)	1.47(3)	C(11)	−0.13(3)
As(2)	1.43(3)	C(12)	−0.04(4)
Co(1)	0.04(1)	C(13)	−0.04(4)
Co(2)	0.16(1)	C(14)	−0.15(4)
O(1)	0.16(8)	C(15)	−0.26(4)
C(1)	−0.17(9)	C(16)	−0.10(4)

Deformation Maps versus Topological Analysis of $\rho(\mathbf{r})$

As discussed in the Introduction deformation density maps are ambiguously flat as far as MM interactions are concerned. Indeed, $Co_2(CO)_6(AsPh_3)_2$ $\Delta\rho(\mathbf{r})$ maps (see Figure 2a,b) show a lack of charge concentration along the MM bond, while both Co−As and Co−C bonds result in accumulation of deformation density. Inadequacies in the description of the metal−metal bond are easily understood by looking at the d-electron density. The occupancy order[36] in Table 2 agrees well with the expected splitting of d orbitals in a trigonal bipyramidal environment, with d_{xz} and d_{yz} overpopulated and d_{z^2} depopulated with respect to a spherically averaged $4s^23d^7$ configuration (the z axis is aligned with the Co−Co bond). Thus the deformation map is characterized by the positive lobes, corresponding to d_{xz} and d_{yz} densities and by a negative region along the Co−Co bond (corresponding to d_{z^2}). The weak π-acceptor power of the arsine ligand is revealed by the positive multipolar charge found on As atoms (see Table 3).

On the other hand, according to QTAM, two atoms are bonded if there exists a maximum electron density path (*bond path*) linking them, which implies a (3,−1) critical point of $\rho(\mathbf{r})$, called *bond critical point* (bcp, $\mathbf{r}_b$). In particular, MacDougall et al.[11a,13] and Bo et al.[14,37] found bond paths and bcp's in unsupported but not in carbonyl bridged metal dimers. Recently, these theoretical predictions have been validated experimentally for $Mn_2(CO)_{10}$,[15] and in close agreement, we have also found a bond path linking the two metal atoms in $Co_2(CO)_6(AsPh3)_2$.

All other expected bond paths and critical points (corresponding to Co−C, Co−As, C−O, As−C, C−C, and C−H bonds)

(28) Hirshfeld, F. *Acta Crystallogr.* **1976**, *A32*, 239−244.

(29) See also: Smith, G. T.; Mallinson, P. R.; Frampton, C. S.; Farrugia, L. J.; Peacock, R. D.; Howard, J. A. K. *J. Am. Chem. Soc.* **1997**, *119*, 5028−5034.

(30) Koritsanszky, T.; Howard, S. T.; Su, Z.; Mallinson, P. R.; Richter, T.; Hansen, N. K. *XD, Computer Program Package for Multipole refinement and Analysis of Electron Densities from Diffraction Data*; Free University of Berlin: Berlin, Germany, June 1997.

(31) (a) In Abramov (Abramov, Y. A. *Acta Crystallogr.* **1997**, *A53*, 264−272), the kinetic energy density at the bond critical point is estimated by $G(\mathbf{r}_b) = (3/10)(3\pi^2)^{2/3}\rho(\mathbf{r}_b)^{5/3} + (1/6)\nabla^2\rho(\mathbf{r}_b)$ (eq 1) (all quantities must be expressed in atomic units). However, for interactions dominated by large orbital overlapping, the best approximation is $G(\mathbf{r}_b) = (3/10)(3\pi^2)^{2/3}(\Delta\rho(\mathbf{r}_b)^{5/3} + \rho_{hyb}(\mathbf{r}_b)^{5/3}) + (1/6)\nabla^2\rho(\mathbf{r}_b)$ (eq 2), where $\Delta\rho(\mathbf{r}_b)$ and $\rho_{hyb}(\mathbf{r}_b)$ are obtained by taking into account a proper promolecule which depends on the atomic hybridization; of course, when the asphericity of the total density is rather small, eq 2 is equivalent to eq 1. In Table 4, the values of $G(\mathbf{r}_b)$ reported have been estimated by eq 1, except those of C−C and C−H bonds, for which eq 2 has been adopted using the appropriate partitioning of sp^2 carbons. The potential energy density, $V(\mathbf{r})$, and the total energy density, $H(\mathbf{r}) = G(\mathbf{r}) + V(\mathbf{r})$, can be obtained by taking into account the local virial theorem, $(\hbar^2/4m)\nabla^2\rho(\mathbf{r}) = 2G(\mathbf{r}) + V(\mathbf{r})$. (b) An application of Abramov's method has also been published in Espinosa et al.: Espinosa, E.; Molins, E.; Lecomte, C. *Chem. Phys. Lett.* **1998**, *285*, 170−173.

(32) (a) Becke, A. D. *J. Chem. Phys.* **1993**, *98*, 5648−5652. (b) Lee, C.; Yang, W.; Parr, R. G. *Phys. Rev.* **1988**, *B37*, 785−789.

(33) Frisch, M. J.; Trucks, G. W.; Schlegel, H. B.; Gill, P. M. W.; Johnson, B. G.; Robb, M. A.; Cheeseman, J. R.; Keith, T.; Petersson, G. A.; Montgomery, J. A.; Raghavachari, K.; Al-Laham, M. A.; Zakrzewski, V. G.; Ortiz, J. V.; Foresman, J. B.; Peng, C. Y.; Ayala, P. Y.; Chen, W.; Wong, M. W.; Andres, J. L.; Replogle, E. S.; Gomperts, R.; Martin, R. L.; Fox, D. J.; Binkley, J. S.; Defrees, D. J.; Baker, J.; Stewart, J. P.; Head-Gordon, M.; Gonzalez, C.; Pople, J. A. Gaussian, Inc., Pittsburgh, PA, 1995.

(34) (a) Hay, P. J.; Wadt, W. R. *J. Chem. Phys.* **1985**, *82*, 270−284. (b) Wadt, W. R.; Hay, P. J. *J. Chem. Phys.* **1985**, *82*, 284−299.

(35) Biegler-König, F. W.; Bader, R. F. W.; Ting-Hua, T. *J. Comput. Chem.* **1982**, *3*, 317−328.

(36) Holladay, A.; Leung, P.; Coppens, P. *Acta Crystallogr.* **1983**, *A39*, 377−387.

(37) Bo, C.; Poblet, J. M.; Benard, M. *Chem. Phys. Lett.* **1990**, *169*, 89−96.

Table 4. Results of the Experimental and Theoretical (B3LYP/6-311+G* on $Co_2(CO)_6(AsH_3)_2$ in S_6 Symmetry) Topological Analysis[a]

bond		d	d_1	$\rho(\mathbf{r}_b)$	$L(\mathbf{r}_b) = -\nabla^2\rho(\mathbf{r}_b)$	ϵ	$G(\mathbf{r}_b)$	$G(\mathbf{r}_b)/\rho(\mathbf{r}_b)$	$H(\mathbf{r}_b)$
Co−Co									
theor		2.64	1.320	0.271	−0.043	0.00	0.093 (0.095)	0.34 (0.35)	−0.090 (−0.093)
expt		2.6430(2)	1.323	0.204(11)	−1.344(8)	0.00	0.120	0.59	−0.025
Co−As									
theor		2.29	1.040	0.518	−3.844	0.00	0.448 (0.417)	0.86 (0.80)	−0.179 (−0.148)
expt	Co1−As1	2.2949(2)	1.083	0.446(11)	−4.25(2)	0.00	0.408	0.91	−0.125
	Co2−As2	2.2906(2)	1.076	0.479(12)	−4.21(2)	0.00	0.432	0.90	−0.138
Co−C									
theor		1.79	0.913	1.005	−13.727	0.02	1.452 (1.354)	1.44 (1.35)	−0.491 (−0.392)
expt	Co1−C1	1.789(1)	0.934	0.930(16)	−12.23(2)	0.04	1.283	1.38	−0.427
	Co2−C2	1.790(1)	0.933	0.921(16)	−12.27(2)	0.02	1.274	1.38	−0.415
C−O									
theor		1.15	0.392	3.126	−10.278	0.01	5.852 (6.175)	1.87 (1.97)	−5.133 (−5.453)
expt	C1−O1	1.153(1)	0.403	3.38(7)	28.8(3)	0.04	4.796	1.42	−6.815
	C2−O2	1.151(1)	0.403	3.39(7)	28.2(3)	0.04	4.843	1.43	−6.819
As−C									
expt	As1−C11	1.940(1)	0.977	0.850(12)	−1.907(9)	0.56	0.702	0.82	−0.569
	As2−C21	1.940(1)	0.956	0.804(8)	−3.594(9)	0.34	0.727	0.90	−0.475
av C−C (expt)		1.398(5)		2.13(6)	19.8(1.3)	0.23(4)	1.02(2)	0.48	−2.41(2)
av C−H (expt)		1.06(3)	0.67(3)	1.94(10)	19(3)	0.10(4)	0.74(13)	0.38	−2.1(3)
av H···O (expt)		2.59(3)	1.10(1)	0.040(4)	−0.70(1)	0.23(4)	0.036(3)	0.90	0.013(2)

[a] For each bond, d is the atomic distance (Å); d_1 is the distance of atom 1 from the bcp; $\rho(\mathbf{r}_b)$ is expressed in e Å^{-3} and $L(\mathbf{r}_b)$ in e Å^{-5}; ϵ is the bond ellipticity; the experimental $G(\mathbf{r}_b)$ and $H(\mathbf{r}_b)$ (hartree Å^{-3}) are computed using Abramov formula,[31a] while for the theoretical ones, we report both the correct $G(\mathbf{r}_b)$ and $H(\mathbf{r}_b)$ (in parentheses) and those obtained applying Abramov approximations.[31a] For d, $\rho(\mathbf{r}_b)$ and $L(\mathbf{r}_b)$, the standard uncertainties (or the deviation from the mean value, whenever an average number is tabulated) are reported in parentheses.

are found together with one ring critical point inside each phenyl. Bond critical points are also found for four independent C−H···O intermolecular interactions, while no bcp was located for intramolecular "face-on" C−H···Ph contacts. The main results of the topological analysis of $\rho(\mathbf{r})$ are summarized in Table 4.

The role of 1,3 M···CO interactions in stabilizing the unsupported MM bond was stressed on the basis of Mulliken populations and energy considerations[2] but was de-emphasized through DD maps[3] and molecular orbitals composition analysis[11,38] and eventually dismissed by QTAM analysis. Accordingly, we did not find, for the title compound, any bcp between Co atoms and the vicinal carbonyls; however, possible evidence of some CO contribution may be found in the shape of the Co−C bond path which is more bent toward the opposite Co than the internuclear vector,[39] suggesting the presence of some overlap between carbonyls π and metal d_{z^2} orbitals.

Usage of the Laplacian for Characterizing M−M and M−L Bonds

As pointed out by Bader and co-workers,[40] the function $L(\mathbf{r}) = -\nabla^2\rho(\mathbf{r})$ of an isolated ground-state atom[41] reproduces the electronic shell structure by alternating a positive and a negative region (containing a maximum and a minimum, respectively) for each shell.[42] However, heavy atoms are known to deviate from this behavior:[43] for instance, fourth-row elements, from Sc to Ge, do not show the expected maxima and minima corresponding to the N shell (which is thus not distinguishable from the M shell) but, starting from As (up to Kr), M and N shells are again separated even if the outermost maxima do not necessarily have $L(\mathbf{r}) > 0$ (see Figure 3). Similar trends are also shown by elements of the successive rows[44] and have been imputed to the diffuse character of the outermost electrons when the atomic core is large.[13b]

When a chemical bond is formed, the $L(\mathbf{r})$ distribution is no longer spherical and its properties are widely used for characterizing atomic interactions since the Laplacian enhances the features of charge distribution and of electron pair localization, providing a physical connection with the classical Lewis model and the valence shell electron pair repulsion theory. The species investigated here, $Co_2(CO)_6(AsPh3)_2$, provides an example for several bond types, which are discussed in the following, also on the basis of examples known in the literature.[6]

When two second-row atoms are covalently bonded, two *valence shell charge concentrations* (VSCC, maxima in $L(\mathbf{r})$[45]) are found along the bond path, one for each atom. A saddle point [(3,−1) critical point of $L(\mathbf{r})$] is nearly coincident with the bcp [(3,−1) critical point of $\rho(\mathbf{r})$]: both have a positive curvature along the bond path line (being minima only along this direction). Since the outermost shells of the two bonded atoms partially overlap, these interactions are *open shell* (or *shared*). At the bcp, the potential energy density ($V(\mathbf{r})$, a negative function everywhere) dominates over the kinetic energy density ($G(\mathbf{r})$, positive everywhere); thus, the total energy density ($H(\mathbf{r}) = V(\mathbf{r}) + G(\mathbf{r})$) is largely negative.[46] Moreover, $\rho(\mathbf{r}_b)$ is large, $L(\mathbf{r}_b) > 0$, and the ratio $G(\mathbf{r}_b)/\rho(\mathbf{r}_b)$ is small. In the title compound, only the phenyl C−C and C−H bonds fall into this class (see Figure 4 and Table 4, where theoretical and

(38) Veillard, A.; Rohmer, M. M. *Int. J. Quantum Chem.* **1992**, *42*, 965−976.

(39) In fact, the two Co−Co−C geometrical angles are 86.8° and 85.4°, while the bond path angles are 86.1° and 84.7°, respectively.

(40) (a) Bader, R. F. W.; Essen, H. *J. Chem. Phys.* **1984**, *80*, 1943−1960. (b) Bader, R. F. W.; MacDougall, P. J.; Lau, C. D. H. *J. Am. Chem. Soc.* **1984**, *106*, 1594−1605.

(41) Based on the Clementi and Roetti HF wave function with atoms in the ground-state configuration.

(42) The actual physical meaning of this feature has been widely discussed in the past few years; however, it has been demonstrated that none of the critical points of $L(\mathbf{r})$ (minima and maxima) nor the zeros can reproduce the expected number of electrons within a given shell (see: Schmider, H.; Sagar, R. P.; Smith, V. H. *J. Chem. Phys.* **1991**, *94*, 8627−8629). Thus, $L(\mathbf{r})$ is a better qualitative index of atomic shells occurrence (with respect to D(r), which also lacks of local maxima for the outermost shells) but is a worse quantitative index (see, for comparison: Sen, K. D.; Slamet, M.; Sahni, V. *Chem. Phys. Lett.* **1993**, *205*, 313−316).

(43) (a) Sagar, R. P.; Ku, A. C. T.; Smith, V. H.; Simas, A. M. *J. Chem. Phys.* **1988**, *88*, 4367−4374. (b) Shi, Z.; Boyd, R. J. *J. Chem. Phys.* **1988**, *88*, 4375−4377.

(44) The maximum number of distinguishable shells is five (see ref 43a).

(45) Formally, a VSCC is found when a $L(\mathbf{r})$ maximum occurs with $L(\mathbf{r}) > 0$.

(46) (a) As demonstrated in Cremer et al. (Cremer, D.; Kraka, E. *Croat. Chem. Acta* **1984**, *57*, 1259−1281), the sign of the energy density computed at the bcp is an index of the amount of covalency in the chemical interaction. (b) See also: Cremer, D.; Kraka, E. *Angew. Chem., Int. Engl. Ed.* **1984**, *23*, 67−68.

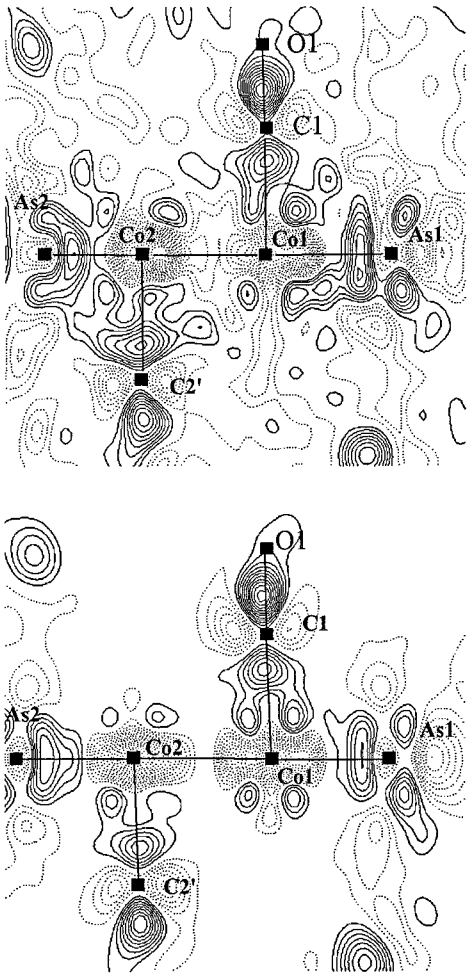

Figure 2. Experimental (a) and model (b) deformation density maps[8] in the plane containing Co1, Co2, As1, and C1 (contour levels are drawn at ± 0.05 e Å^{-3}; positive levels are solid lines). Note the absence of charge accumulation in the intermetallic region in contrast to metal−ligand zones and the appearance of excess density in the d_{xz} and d_{yz} orbitals of the metals.

experimental results are compared; in particular, the semiempirical expression proposed by Abramov[31a] for obtaining the kinetic energy density is tested).

When the bond is ionic, as in NaCl, the outermost shell of the cation is totally superimposed to that of the anion and, along the bond path, one cannot distinguish [in $L(\mathbf{r})$] the M shell of Na which is "hidden" by that of Cl. The bcp is shifted toward Na and lies in a large and flat negative region of $L(\mathbf{r})$ where the total amount of density is small. Due to the electron transfer, the electronic configurations of Cl and Na are now, formally, those of Ar (= Cl^-) and Ne (= Na^+), see Figure 5; as a consequence, these interactions are called *closed shell*. The kinetic energy density here dominates over the potential energy density (thus, $H(\mathbf{r}_b) > 0$ and $G(\mathbf{r}_b)/\rho(\mathbf{r}_b) \gg 1$). Bader has discussed other closed-shell interactions, such as hydrogen bonds, and all share a common "fingerprint": $L(\mathbf{r}_b) < 0$ (the bcp lying close to a $L(\mathbf{r})$ maximum along the bond path direction),[47] $\rho(\mathbf{r}_b)$ small, $H(\mathbf{r}_b) > 0$, and $G(\mathbf{r}_b)/\rho(\mathbf{r}_b) \sim 1$, as we have found here for the weak C−H···O bonds (see Table 4 and Figure 4).

The closed-shell vs open-shell classification based on the sign of $L(\mathbf{r}_b)$ is much simplified when the bcp lies far from the nodal surfaces of the Laplacian[6] (as in the previous examples), while *intermediate interactions* must be invoked when the bcp is close to such boundaries. When the bond is shared but polarized, the bcp is shifted toward the VSCC of one of the two atoms (the less electronegative)[48] and eventually both VSCC's belong to the basin of the more electronegative atom.[49] For instance, in free CO, the bcp is so close to C (0.374 Å) that $L(\mathbf{r}_b) < 0$; in the title compound, theoretical and experimental topology agree in shifting the bcp of C−O bonds toward oxygen, with respect to the isolated CO, but they slightly disagree in the extent of such shift, thus experimentally $L(\mathbf{r}_b) > 0$ (since the shift is larger), while theoretically $L(\mathbf{r}_b) < 0$[50] (see Table 4 and Figures 4 and 6). The strong polar character is revealed by a large $G(\mathbf{r}_b)/\rho(\mathbf{r}_b)$ ratio coupled to a negative $H(\mathbf{r}_b)$ and a large $\rho(\mathbf{r}_b)$. In donor−acceptor bonds (as in OC|→BH_3),[51] a unique VSCC, corresponding to the lone pair of the nucleophilic atom (carbon), and a charge depletion, on the electrophilic one (boron), are found along the bond path; the bcp is shifted toward the acceptor, but it cannot be associated to any critical point of $L(\mathbf{r})$ (since B has lost its VSCC). This kind of interactions is characterized by relatively large $\rho(\mathbf{r}_b)$, negative $H(\mathbf{r}_b)$, $G(\mathbf{r}_b)/\rho(\mathbf{r}_b) > 1$, and $L(\mathbf{r_b}) < 0$, in agreement with what is here found for the Co−CO bonds (Figure 4 and Table 4).

Due to the "anomalous" distribution of shell maxima and minima and to the atomic-size effect, heavy atom−heavy atom bonds (HH, we call heavy atoms those with more than three atomic shells) and heavy atom−light atom bonds (HL) have different features in the Laplacian distribution than light atom−light atom (LL) bonds and the shared or closed-shell character is not easily assignable. In $Co_2(CO)_6(AsPh_3)_2$, for instance, there are two kinds of HH bond, Co−Co and Co−As, both having $L(\mathbf{r}_b) < 0$ and small $\rho(\mathbf{r}_b)$ as in LL closed-shell interactions, although we expect the former to behave as a shared and the latter as a donor−acceptor bond.[52]

A closer inspection of $L(\mathbf{r})$ distribution along the bond path shows that in Co−Co the bcp is located on a $L(\mathbf{r})$ maximum produced by the condensation of the two vanishing N shells, a feature first observed by MacDougall[13] for $Mn_2(CO)_{10}$.[53] It is worth noting that this situation is somewhat similar to that of F_2[6,13a,46b] and, even more, to that of B_2 (see Figure 5);[54] in agreement, the potential energy density is still dominating at the bcp (thus $H(\mathbf{r}_b) < 0$) and the total amount of kinetic energy density is small ($G(\mathbf{r}_b)/\rho(\mathbf{r}_b) < 1$). Moreover, despite the small $\rho(\mathbf{r}_b)$, the Co−Co interaction is not necessarily weak; in fact, it has been suggested that only the integrated density, over the whole zero-flux surface separating two bonded atoms, provides meaningful results when diffuse electrons contribute to the

(47) For very short hydrogen bonds, the interaction is actually shared and $L(\mathbf{r_b}) > 0$. See, for instance: Flensburg, C.; Larsen, S.; Stewart, R. F. *J. Phys. Chem.* **1995**, *99*, 10134−10141.

(48) A few years ago, there was a discussion about the actual effect of the so-called atomic orbital size in producing this shift. See: (a) Perrin, C. L. *J. Am. Chem. Soc.* **1991**, *113*, 2865−2868. (b) Gatti, C.; Fantucci, P. *J. Phys. Chem.* **1993**, *97*, 11677−11680.

(49) The shift between the (3,−1) point in $L(\mathbf{r})$ and bcp can be used as an index for the polarity of the bond.

(50) Moreover, experimentally a VSCC on C along C−O bond is found, while theoretically it is lacking (as in free CO); visually judging, also the experimental $L(\mathbf{r})$ of $Mn_2(CO)_{10}$ shows VSCCs on carbonyl carbons (see Figure 2b of ref 15) which are not observed theoretically (refs 13 and 14).

(51) Volker, J.; Frenking, G.; Reetz, M. T. *J. Am. Chem. Soc.* **1994**, *116*, 8741−8753.

(52) Even M−M quadruple bonds have (theoretical) $L(\mathbf{r}_b) < 0$ despite the large and $\rho(\mathbf{r}_b)$ (see: Sierraalta, A. *Chem. Phys. Lett.* **1994**, *227*, 557−560).

(53) Note, however, that the sign of $L(\mathbf{r}_b)$ strongly depends on the basis set employed.

(54) In B−B a "contracted" double maximum with a saddle point can be observed at the bcp, while for F_2, in addition to the $L(\mathbf{r})$ maxima of the two valence shells, there is also a $L(\mathbf{r})$ maximum inside the bond. Thus Co−Co is much more similar to Li−Li or B−B bonds.

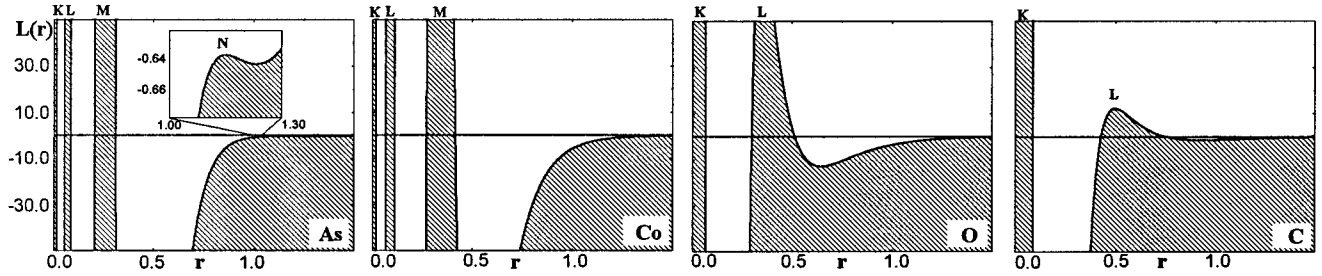

Figure 3. $L(\mathbf{r})$ of the spherically averaged density for As, Co, O, and C atoms (computed from Clementi and Roetti[24] atomic HF wave functions); note the lack of the N shell of Co and the "hidden" maximum of As N shell, which occurs at $L(\mathbf{r}) < 0$ (the atomic radii are in Å and L(r) in e Å^{-5}).

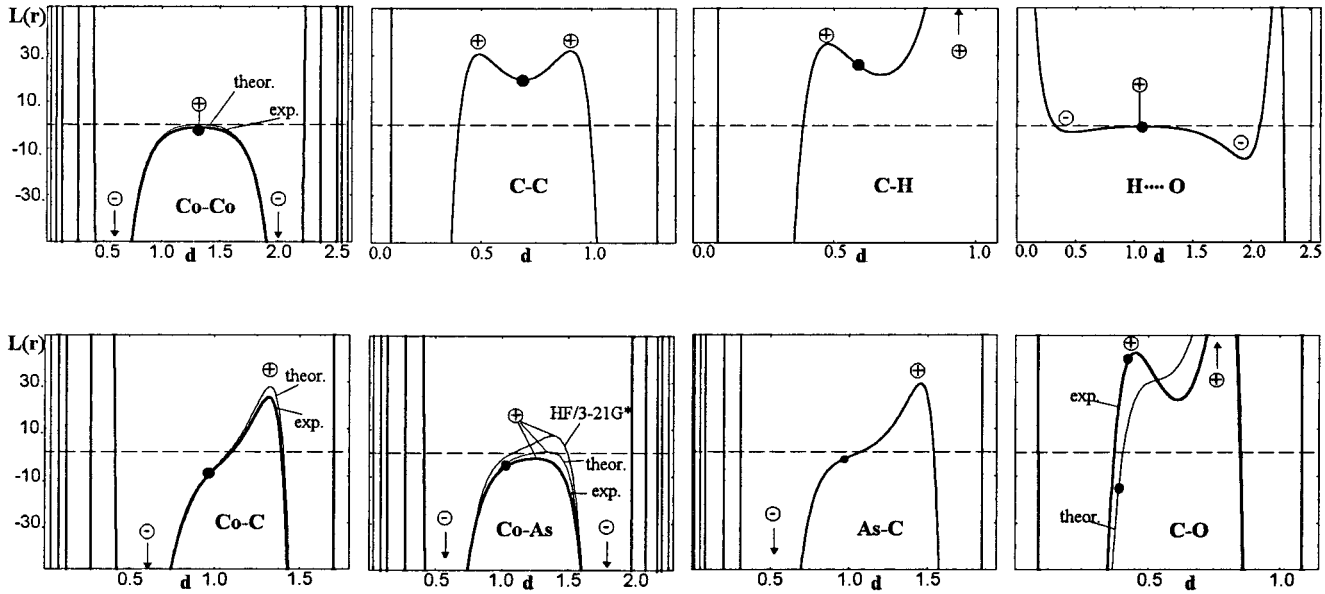

Figure 4. Experimental $L(\mathbf{r})$ distribution along the bond paths (distances are in Å and $L(\mathbf{r})$ in e Å^{-5}). The positions of bcp (filled dot) and of $L(\mathbf{r})$ maxima and minima (+ and −, respectively) are reported. The profiles obtained by theoretical calculations (B3LYP/6-311+G*) are also shown; the qualitative agreement is in general good, except for the C−O bond. Note the effect of the basis set choice which is qualitatively relevant for Co−As (other basis sets produced intermediate profiles).

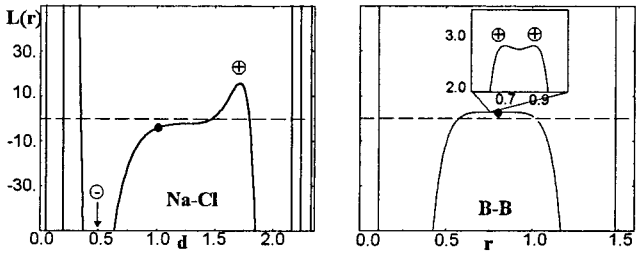

Figure 5. $L(\mathbf{r})$ distribution along the bond paths of Na−Cl and B−B bonds.[6]

bond[46] (a typical example is provided by Li_2).[55] Hence, the Co−Co bond is far from the closed-shell limit and we do not find any reason for not considering it a *shared* interaction as suggested by common chemical sense.[56] Note that similar features for MM bonds were found in heterobinuclear dimers,

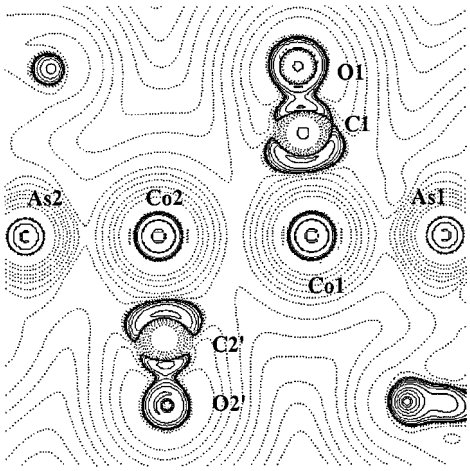

Figure 6. $L(\mathbf{r})$ distribution in the same plane of Figure 2 (contour levels at 2.0×10^x, 4.0×10^x, and 8.0×10^x e Å^{-5}, $x = -2, -1, 0, +1$; positive $L(\mathbf{r})$ are solid lines).

where some polar metallic bonds have been characterized by comparing different theoretical approaches[57] (QTAM, charge decomposition analysis, natural population analysis, and electron localization function), and in metals or alloys,[58] where the curvature components of the density have a rather small magnitude at the bcp and $L(\mathbf{r}_b) < 0$.

In the Co−As bond, the bcp is shifted toward Co and located between a maximum, belonging to As, and a minimum (on Co)

(55) In ref 46a $\rho(\mathbf{r}_b)$ for Li−Li bond is 0.083 e Å^{-3}, while the density integrated over the zero-flux surface is 0.743 e Å^{-1} (which represents one of the largest differences among chemical bonds investigated so far).

(56) Theoretical calculations (refs 13, 14, and 37) showed that $L(\mathbf{r})$ in transition metal complexes displays peculiar shapes fully consistent with the ligand field theory. Here, the theoretical $L(\mathbf{r})$ (unrespective of the basis set employed) shows the features expected for a trigonal bypiramidal metal coordination (ref 13), i.e. six inner VSCC disposed as a trigonal prism around Co (which are also found in the experimental $L(\mathbf{r})$), whose five faces are "centered" by $L(\mathbf{r})$ minima pointing toward the five bonding directions (three of them being only (3,−1) critical points in the experimental $L(\mathbf{r})$, possibly because the tangential curvatures of L(**r**) are small and largelly affected by experimental errors).

Table 5. Summary of the Features Which Characterize the Atomic Interactions

	$\rho(\mathbf{r}_b)$	position of $\mathbf{r}_b$ with respect to $L(\mathbf{r})$ along the bond path	$L(\mathbf{r}_b)$	$G(\mathbf{r}_b)/\rho(\mathbf{r}_b)$	$H(\mathbf{r}_b)$
		LL bonds			
open-shell (covalent bonds, e.g. C−C, C−H, B−B)	large	close to a minimum	>0	<1	<0
intermediate interactions ("polar shared" bonds, e.g. CO)	large	close to a nodal surface	arbitrary	≥1	<0
closed-shell (ionic bonds, hydrogen bonds, van der Waals interactions, e.g. NaCl, H···O)	small	inside a flat region	<0	≥1	>0
		HH bonds			
shared (e.g., Co−Co)	small	close to a maximum	∼0	<1	<0
donor−acceptor (e.g., Co−As)	small	close to a nodal surface	<0	∼1	<0

of $L(\mathbf{r})$ (see Figure 4). These features "topologically" parallel those of the Co−C interaction (where the unique $L(\mathbf{r})$ maximum belongs to C), though $H(\mathbf{r}_b)$, $G(\mathbf{r}_b)/\rho(\mathbf{r}_b)$, and the shape of $L(\mathbf{r})$ differentiate the two ligands. The distinction between the donor−acceptor Co−As and the shared Co−Co bond is subtler than that between the corresponding LL interactions.

Finally, we note that the As−C bonds appear, judging from the shape of $L(\mathbf{r})$, as highly polar-shared interactions, while they should be only weakly polar (as also indicated by the $G(\mathbf{r}_b)/\rho(\mathbf{r}_b)$ ratio which is definitely smaller than that of C−O bonds); as a matter of fact, the loss of the valence shell of the less electronegative atom is here enhanced by the intrinsic VSCC shape of atomic As (which, besides occurring at negative $L(\mathbf{r})$, is only a ripple; see Figure 3).

The main features of each kind of interaction described are resumed in Table 5.

Conclusions

The major outcomes of this paper are the experimental proof of the presence of a genuine, covalent Co−Co bond, the warnings on the usage of $L(\mathbf{r}_b)$ *only* as an *absolute* index of the nature of chemical bonds, and the attention given to the shape and the topology of $L(\mathbf{r})$ along the bond path (as determined by specific *atomic* characters, such as the nature of the valence shell orbitals, core size effects, and electronegativity).

When at least one heavy atom is concerned, the radial shape of the atomic $L(\mathbf{r})$ makes the character of the interaction less clearly defined and the inspection of the other critical parameters, like $H(\mathbf{r}_b)$, $G(\mathbf{r}_b)/\rho(\mathbf{r}_b)$, and the position of $\mathbf{r}_b$, is required. However, even if it is possible to recognize the shared character of Co−Co and As−C bonds if compared with the donor−acceptor Co−As and Co−C distinctions and similarities are sometimes grounded on subtleties which could hardly suffice without some a priori chemical insight. On the contrary, the same distinctions are much easier for LL bonds where critical parameters convey, unambiguously, the right information. Moreover, although a separation between heavy and light atom behaviors has been here proposed, it is worth noting that properties shown by heavy atoms are *in pectore* recognizable[59] also in early elements of the first three rows:[6,43b] in fact, the Co−Co bond shows strict similarities with the B−B one (i.e., the small $\rho(\mathbf{r}_b)$, the small $G(\mathbf{r}_b)/\rho(\mathbf{r}_b)$, the negative $H(\mathbf{r}_b)$, and the shape of $L(\mathbf{r})$ along the bond path).

The semiempirical method proposed by Abramov[31a] has been here adopted for computing experimentally $G(\mathbf{r}_b)$ and, consequently, $H(\mathbf{r}_b)$, which are important descriptors of the atomic interactions, widely used by theoreticians and particularly useful for bonds dominated by charge depletion, as usually occurs for HH and HL bonds. Most of the experimentally determined properties have been verified against theoretical calculations on the idealized $Co_2(CO)_6(AsH_3)_2$ molecule, showing a favorable agreement (but for C−O bonds), besides the intrinsic differences between the two approaches. Theoretical $\rho(\mathbf{r})$'s, obtained from molecular orbital wave functions, suffer from basis set limitations (usually far from the HF quality)[60] and the neglect of electron correlation (which, in large molecular systems, can be taken only partially into account) but are free from experimental errors and molecular motions. On their hand, experimental electron densities take advantage of the usage of atomic Slater Hartree−Fock (HF) wave functions and by some implicit modeling of electron correlation, though the flexibility of the deformation functions can hardly exceed the hexadecapolar level. At present, the only way to obtain experimental densities and Laplacian distributions unbiased by the wave function choice[61] is the usage of maximum entropy methods.[62] Both experimental and theoretical densities are usually limited by the neglect of relativistic effects.[63]

Given this situation, we think that theory and experiment are complementary and we plan soon to better characterize larger molecules, such as low-nuclearity transition metal clusters, coupling the two approaches.

Acknowledgment. The authors thank the Dipartimento di Chimica Fisica ed Elettrochimica (Università di Milano) for providing computer time and software supports. Prof. L. Garlaschelli is thanked for synthesizing and crystallizing the title compound.

Supporting Information Available: Full table of coordinates, anisotropic thermal parameters, bond distances, and multipolar populations parameters (9 pages). See any current masthead page for ordering information and Web access instructions.

JA982903M

(57) Jansen, G.; Schubart, M:; Findeis, B.; Gade, L. H.; Scowen, I.; McPartlin, M. *J. Am. Chem. Soc.* **1998**, *120*, 7239−7251.

(58) Eberhart, M. E.; Donovan, M., M.; Outlaw, R. A. *Phys. Rev. B* **1992**, *46*, 12744−12747.

(59) I.e., present in part but not fully manifested.

(60) In ref 43b, significantly qualitative differences were obtained when single-ζ or double-ζ Slater orbitals are used instead of the full HF expansion of Clementi and Roetti. Moreover, the usage of pseudo-potentials lead to relevant discrepancies when correct Laplacian distributions are compared (Kohout, M.; Savin, A.; Preuss, H. *J. Chem. Phys.* **1991**, *95*, 1928−1942).

(61) In principle, the exact $\rho(\mathbf{r})$ and $\nabla^2\rho(\mathbf{r})$ should be available through Fourier summation, but series termination contaminates $\rho(\mathbf{r})$ and more heavily $\nabla^2\rho(\mathbf{r})$. See: (a) Stewart, R. F. *The application of charge density research to chemistry and drug design*; Jeffrey, A. G., Piniella, J. F., Eds.; Plenum Press: New York, 1991. (b) Stewart, R. F. *Chem. Phys. Lett.* **1979**, *65*, 335−342.

(62) Efforts to calculate $L(\mathbf{r})$ with MEM will be reported in due course (Roversi, P. personal communication).

(63) However, X-ray scattering factors computed from Dirac−Fock multiconfiguration wave functions are now available. See: (a) Su, Z.; Coppens, P. *Acta Crystallogr.* **1997**, *A53*, 749−762. (b) Wang, J.; Smith, V. H.; Bunge, C. F.; Jauregui, R. *Acta Crystallogr.* **1996**, *A52*, 649−658.